Communications in Physics, Vol. 30, No. 3 (2020), pp. 257-266
DOI:10.15625/0868-3166/30/3/14882

EFFECT OF Sm AND Mn CO-DOPING ON THE CRYSTAL STRUCTURE AND MAGNETIC PROPERTIES OF $BiFeO_3$ POLYCRYSTALLINE CERAMICS

NGUYEN VAN HAO[1], PHAM VAN HAI[2], TRUONG THI THAO[3],
NGUYEN THI MINH HONG[4] AND PHAM TRUONG THO[1,†]

[1]*Department of Physics and Technology, TNU-University of Sciences, Thai Nguyen, Vietnam*
[2]*Department of Physics, Hanoi National University of Education, 136 Xuan Thuy, Hanoi, Vietnam*
[3]*Department of Chemistry, TNU-University of Sciences, Thai Nguyen, Vietnam*
[4]*Faculty of Engineering Physics and Nanotechnology,*
VNU University of Engineering and Technology, Hanoi, Vietnam

[†]*E-mail:* thopt@tnus.edu.vn

Received 10 March 2020
Accepted for publication 16 June 2020
Published 23 July 2020

Abstract. *The crystal structure, phonon vibration, microstructure, and magnetic properties have been investigated in multiferroics $Bi_{0.9}Sm_{0.1}Fe_{1-x}Mn_xO_3$ for $x = 0.02 - 0.1$. The structural analysis by XRD and Rietveld refinement suggests that Mn doping compounds crystallize in the polar R3c rhombohedral symmetry (isostructural with $BiFeO_3$). Raman analysis confirms no structural transformation but the change of line widths and peak intensities reveal the lattice distortion in Mn-substitution samples. The study of microstructure shows no obvious change of grain size and shape. The magnetic properties of the as-prepared samples show the linear magnetic field dependence of magnetization, suggesting the antiferromagnetic feature of polycrystalline ceramics. The field dependence of magnetization measured after two-years synthesis and after applying an electric field reveal a decrease of maximum magnetization but the hysteresis loops retain the antiferromagnetic behavior. The implication of these results is that the magnetic properties of single structural phase compound, including coercivity and remanent magnetization, do not show the aging behavior as observed in the morphotropic phase boundary systems.*

Keywords: $BiFeO_3$-multiferroics, crystal structure, magnetic properties.

Classification numbers: 61.66.Fn, 75.60.Ej, 75.85.+t.

I. INTRODUCTION

Multiferroic materials that possess a combination of two or more primary ferroic orders in the same phase have continuously extensive study in recent year due to theirs promising application in next-generation multifunction electronic devices [1, 2]. Since most of the known multiferroic materials have a magnetoelectric coupling below room temperature, $BiFeO_3$ is one of the most investigated multiferroic material because it exhibits high ferroelectric Curie temperature of 1103 K and antiferromagnetic Néel temperature of 643 K [3]. At room temperature, $BiFeO_3$ crystalizes in the noncentrosymmetric rhombohedral structure (space group $R3c$) and possesses a large spontaneous polarization $P_S \sim 100\ \mu C/cm^2$ directed along the $[001]_{hex}$ axis [4]. Despite having the large spontaneous polarization of bulk $BiFeO_3$, the magnetoelectric coupling shows very low value with the absence from quadratic term because the cycloidal modulated spin structure cancels a net magnetization arising from the antisymmetric spin coupling (Dzyaloshinskii-Moriya interaction) inside the G-type antiferromagnetic structure [5]. To overcome this obstacle, recent works have focused on chemical substitution in the Bi-site and Fe-site to collapse the space modulated spin structure [6–8]. The substitution of rare-earth elements for $BiFeO_3$ changes the ferroelectric properties and suppresses the cycloidal spin structure to reveal the weak ferromagnetic behavior [9, 10]. Moreover, lanthanide doping also induces a structural transition from the initial antiferromagnetic/polar rhombohedral $R3c$ phase to the weak ferromagnetic/antipolar orthorhombic $PbZrO_3$-like phase and then to the weak ferromagnetic/nonpolar orthorhombic *Pnma* (or *Pbnm*) phase [11]. The thresh hold concentration that induces the polar to antipolar transition in the $Bi_{1-y}Ln_yFeO_3$ (Ln = lanthanide) series depends on the ionic radius of the dopants and sintering temperature, such as $y \sim 0.16$ for La [12], $y \sim 0.11$ for Pr [13], $y \sim 0.12$ for Sm [14]. The structural transformation obviously destroys the spin cycloid as well as ferroelectricity suppression. Therefore, research efforts are now devoted to investigating the magnetic and ferroelectric properties near the morphotropic phase boundary of rhombohedral and orthorhombic phases, where the ferroelectricity and weak ferromagnetism can be simultaneously occurred [15]. In contrast to Bi-site substitution, most of $3d$ transition metals are hardly incorporated in the crystal lattice of $BiFeO_3$ and weakly affects to the spin cycloid [11, 16, 17]. Among the transition metals, manganese substituted $BiFeO_3$ does not alter the initial $R3c$ symmetry up to 30% Mn in place of Fe site; however, it strongly decreases the Curie and Néel temperatures [18]. Although the co-substitution of Sm and Mn has been extensively studied over the years, there are some controversies regarding the crystal structure and magnetic properties of Sm and Mn co-substituted compounds [19–25]. Saxin *et al.* reported that the Mn doped $Bi_{0.9}Sm_{0.1}FeO_3$ can induce the structural transition from the $R3c$ rhombohedral to *Imma* orthorhombic structures at a threshold Mn concentration of 15%. Up to date, the stabilization of the *Imma* phase in the (Sm, Mn) codoped $BiFeO_3$ cannot be reproduced. It is widely known that manganese cannot suppress the cycloidal spin structure in the $R3c$ symmetry. Thus, the observation of weak ferromagnetism in the $Bi_{0.92}Sm_{0.08}Fe_{0.95}Mn_{0.05}O_3$ ceramics is not yet clearly understood [23]. In order to shed some light on the magnetic properties of Sm and Mn co-substituted $BiFeO_3$, we investigate the crystal structure, phonon vibration, microstructure, and magnetic properties of $Bi_{0.9}Sm_{0.1}Fe_{1-x}Mn_xO_3$ ($x = 0.02 - 0.1$) ceramic compounds. We confirm that Mn does not induce the structure transformation in the $Bi_{0.9}Sm_{0.1}Fe_{1-x}Mn_xO_3$ ceramic compounds. The magnetic properties show a clear antiferromagnetic feature with the linear magnetic field dependence of magnetization. The magnetic properties of compounds have been tested

at different characterization time and in an electric field. A decrease of maximum magnetization is observed; but the hysteresis loops retain the antiferromagnetic behavior. The magnetic measurement at different time confirms that the coercivity and remanent magnetization do not show the aging behavior as typically observed in the morphotropic phase boundary systems. The structural defect rearrangement is therefore less influence on the magnetic properties of polycrystalline ceramic samples.

II. EXPERIMENT

Polycrystalline compounds of the form $Bi_{0.9}Sm_{0.1}Fe_{1-x}Mn_xO_3$ (BSFMO) with $x = 0.02$ – 0.1 were synthesized via a conventional solid-state reaction method using high-purity powders of Bi_2O_3, Sm_2O_3, Fe_2O_3, and MnO_2. The powders were weighed in stoichiometry proportions, carefully ground in an agate mortar, and then calcined at 910°C in air for 24 h. Subsequently, the calcined powders samples were re-ground, pressed into pellets, and finally sintered in air at 930°C for 12 h. The crystallinity and phonon characteristics of ceramics were examined using an X-ray diffractometer (Miniflex Rigaku) equipped with a Cu-Kα radiation source ($\lambda = 1.5405$ Å), and Raman scattering spectroscopy (LabRAM HR Evolution, Horiba) with excitation wavelength of $\lambda = 532$ nm. The microstructure was analyzed by using a scanning electron microscope (Hitachi S – 4800). The XRD data were analyzed by the Rietveld method using the GSAS-2 program. Magnetization measurements were performed on a VSM LakeShore 7400. All investigations were carried out at room temperature.

III. RESULTS AND DISCUSSION

The powder XRD patterns of BSFMO samples are shown in Fig. 1. It can be seen that all the samples show high intensity peaks in the presented diffractograms, which implies a good crystallinity of the polycrystalline ceramics. All the diffraction peaks of samples are well indexed as per rhombohedrally distorted perovskite structure of $BiFeO_3$ with a space group of the $R3c$ symmetry [25]. Though the impurity phases, such as $Bi_2Fe_4O_9$ and $Bi_{25}FeO_{40}$, are routinely observed in $BiFeO_3$ due to the volatility of Bi_2O_3 at high sintering temperature [20, 23, 24], no trace of impurity or secondary phase could be distinguished in our samples within the uncertainty of XRD [17]. So, the co-substitution of Sm and Mn can well eliminate the impurity phase, which is in good agreement with rare-earth elements and transition metals co-doped $BiFeO_3$ in the previous works [23, 24, 26].

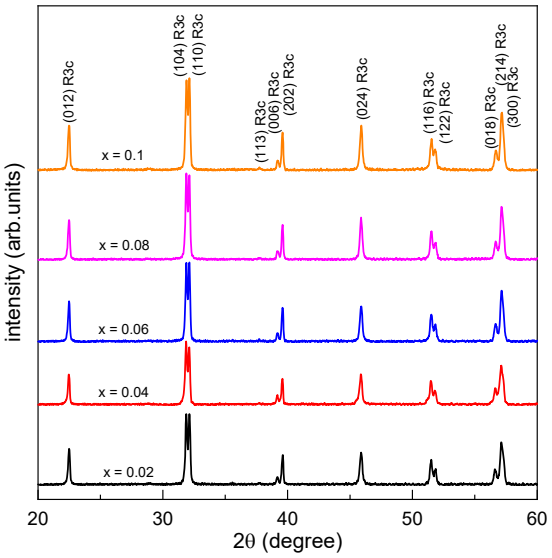

Fig. 1. Powder XRD patterns of BSFMO samples.

It has been reported that the substitution of 10% Mn for $BiFeO_3$ does not induce a structure transformation, but it can reduce the unit cell volume and causes a weakening of the lone-pair activity, leading a diminution of ferroelectricity in Mn doped $BiFeO_3$-based compounds [23, 27, 28]. In the BSFMO compounds, we observe a shift of diffraction peaks towards higher 2θ angle with increasing Mn concentration. This result suggests that Mn doping modifies the $R3c$ rhombohedral symmetry as Sm and Mn incorporated into the crystal structure of $BiFeO_3$. To further confirm the crystal symmetry of BSFMO samples, we refine the diffraction patterns by using the $R3c$ model with the unit cell parameters $a = b = \sqrt{2}a_c$ and $c = 2\sqrt{3}a_c$, where $a_c \approx 4$Å is the parameter of an ideal cubic perovskite. The atomic positions for $x = 0.1$ sample can be seen in Table 1. The typical Rietveld refined XRD patterns for $x = 0.02$ and 0.1 samples are shown in Fig. 2. It is clearly observed that the Rietveld refinement results give a good fit between the experiment and simulation patterns. The calculated crystal symmetry and lattice parameters of BSFMO compounds in Table 2 are well confirmed a slight shrinkage of the $R3c$ rhombohedral unit cell.

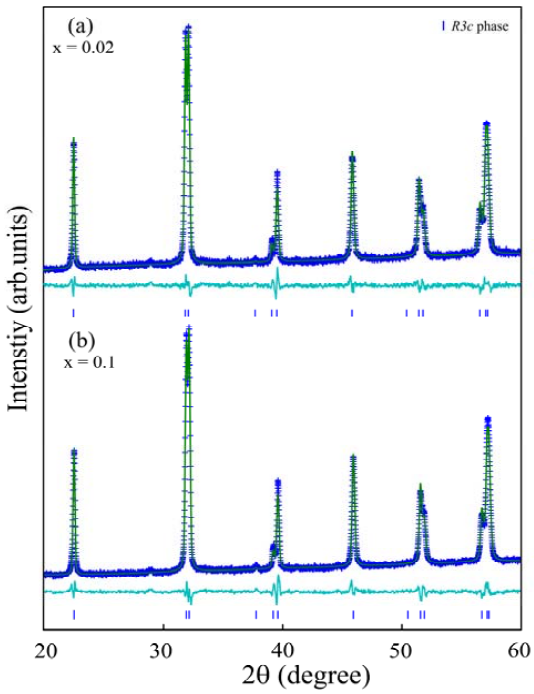

Fig. 2. Rietveld refinement of XRD patterns for (a) $x = 0.02$ and (b) $x = 0.1$.

Table 1. Structural parameters of the $Bi_{0.9}Sm_{0.1}Fe_{0.9}Mn_{0.1}O_3$ compound at room temperature.

Atom	Site	x	y	z	$U_{iso} \times 100$ (Å)	Residuals
Bi/Sm	6a	0	0	0	1.07	GOF = 1.15
Fe/Mn	6a	0	0	0.22446	0.51	wR = 5.14 %
O	18b	0.50516	0.003580	0.94330	1.67	

Table 2. The crystal symmetry and lattice parameters of $Bi_{0.9}Sm_{0.1}Fe_{1-x}Mn_xO_3$ compounds.

Composition	Space group	a(Å)	b(Å)	c(Å)	V(Å)^3
$x = 0.02$	$R3c$	5.5661	5.5661	13.7959	370.16
$x = 0.04$	$R3c$	5.5659	5.5659	13.7903	369.97
$x = 0.06$	$R3c$	5.5658	5.5658	13.7859	369.84
$x = 0.08$	$R3c$	5.5654	5.5654	13.7829	369.72
$x = 0.1$	$R3c$	5.5643	5.5643	13.7781	369.44

Figure 3 shows the Raman spectra of BSFMO sample at room temperature. According to group theory, the Raman modes of the $R3c$ rhombohedral symmetry can be summarized using the irreducible representation: = $4A_1$ + 9E [19]. Due to the angular dispersion of Raman frequency in $BiFeO_3$, the number of phonon active mode can vary from 9E(TO) + $4A_1$(LO) for α = 0 to 9E(LO) + $4A_1$(TO) for $\alpha = \pi/2$, where α is the angle between the incoming laser light and the $[111]_c$ pseudocubic direction [29] Therefore, the Raman modes of bulk $BiFeO_3$ can be assigned to 13TO + 13LO mode frequencies. In present study, we observe nine Raman modes for all samples, which are located at about 136, 170, 229, 256, 278, 375, 476, 523, and 623 cm^{-1}; these modes can be assigned to E-2(TO), E-2(LO), A_1-2(TO), E-4(TO), E-5(TO), E-7(TO), E-8(LO), E-9(TO), and E-9(LO), respectively [30]. The number of Raman modes are independence of Mn concentration, implying that Mn substitution does not alter the structure symmetry of the parent compound ($Bi_{0.9}Sm_{0.1}FeO_3$). As observed in Fig. 3, the intensity of E-2(LO) mode decreases with increasing Mn concentration, while its frequency remains unchanged in all samples. In addition, the E-2(TO) mode clearly shows a blue shift from 136 cm^{-1} for $x = 0.02$ to 138 cm^{-1} for $x = 0.1$. Obviously, the change in intensity of the E-2(LO) and the blue shift of E-2(TO) modes are related to the change of Bi-O covalent bonds induced by Mn-substitution [31]. Thus, the weakening of stereochemical activity of Bi lone electron pair is well concerned with the reduction in intensity of the E-2(LO) mode and the depression of the ferroelectric properties. It is widely known that the frequency of the A_1-2(TO) mode is dependent on the octahedral tilt angle [32], that a slight blue shift of the A_1-2(TO) mode from 229 cm^{-1} for $x = 0.02$ to 234 cm^{-1} for $x = 0.1$ contributes to the rotation of oxygen atoms along [111] axis. The change of octahedral tilt angle possibly affects the magnetic properties of BSFMO compounds [33]. Moreover, it is clearly seen in Fig. 3 that the frequency of other Raman modes does not vary with a change of Mn concentration, but the substitution of Mn at Fe site does influence on peak intensities, especially the intensity of E-9(LO) mode. The change in peak position and intensity well confirms the Mn substitution-driven a structural distortion in BSFMO compounds, which is in good agreement with the analysis of XRD patterns.

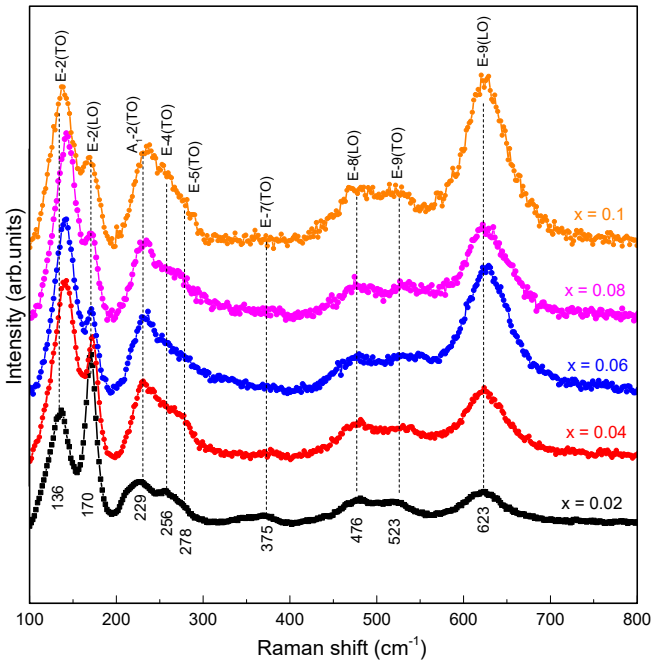

Fig. 3. Raman scattering spectra of BSFMO samples at room temperature.

Figure 4 shows the typical SEM micrographs for $x = 0.02$, 0.06, 0.08, and 0.1 samples. The micrographs show a polygon grain with a random distribution of grain size. The average grain size is around 30-40 μm for all samples and hence the co-substitution of Sm and Mn for $BiFeO_3$ is

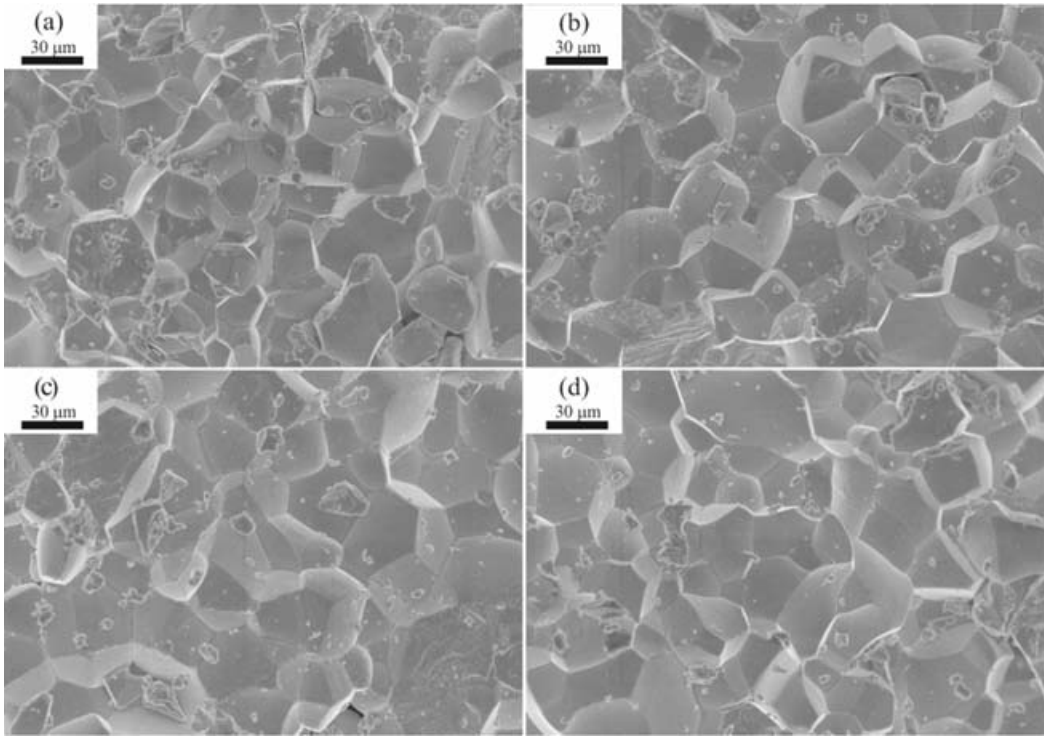

Fig. 4. SEM micrographs of samples (a) $x = 0.02$, (b) $x = 0.06$, (c) $x = 0.08$, and (d) $x = 0.1$.

less effective change the grain size. The significant reduction of grain size is previously observed in the system that have a structural transformation [34]. Thus, the homogeneous grain shape and size distribution are well confirmed no structural transition in BSFMO compounds.

Figure 5 shows the $M - H$ loops of BSFMO samples measured after synthesis. The linear magnetic field dependence of magnetization is observed in all samples, which is similar to the magnetic properties of bulk $BiFeO_3$ [16]. It is known that the cycloidal spin structure superimposed on the G-type antiferromagnetic order cancels the observation of the weak ferromagnetism in $BiFeO_3$ [35] In general, the weak ferromagnetic behavior of $BiFeO_3$-based compounds can be observed by collapse the cycloidal spin modulation The spin cycloid can be manipulated by epitaxial strain [17], chemical substitution [20] or reduced particle size below the cycloid periodicity [36]. The chemical substitution mainly results in a structural distortion and induces a structural transition and hence both of them can unlock the weak ferromagnetism. Obviously, our polycrystalline ceramic samples show a large grain size in μm range, which is much larger than the cycloid periodicity of 62 nm, and no structural transition occurs in our sample. Thus, Mn substitution-induced the structural distortion, which is evidenced by the change in Raman spectra and XRD patterns, possibly changed the magnetic properties. Unfortunately, as observed in Fig. 5, Mn doping cannot be destabilized the cycloidal spin structure of BSFMO compounds, although the octahedral tilt angle is clearly changed, as evidenced from the change of

tilt mode frequency. It is worth to mention that the increase of octahedral tilt angle would enhance the Dzyaloshinskii-Moriya interaction and rises the weak ferromagnetism in antiferromagnetic material [37]. Despite the change of octahedral tilt angle, no change in the magnetic properties of BSFMO compounds is observed, which is unusual phenomenon. The study of Bielecky *et al*. shows that samarium or lanthanum doped $BiFeO_3$ can alter the octahedral tilt angle, but no deviation from linearity of *MH* loops is observed for the $Bi_{0.9}Sm_{0.1}FeO_3$ and $Bi_{0.9}La_{0.1}FeO_3$ compounds [30]. Moreover, the previous reports reveal an argument in the magnetic properties of $Bi_{0.9}Sm_{0.1}FeO_3$ ceramics for which the weak ferromagnetism is observed in Refs. [23, 38], while an intrinsic antiferromagnetic feature of $BiFeO_3$ is observed in Ref. [14]. Therefore, the weak ferromagnetism possibly arises from different sources, such as the suppression of spin cycloid, lattice defection (oxygen vacancy), double exchange interaction of multivalent state of Fe atoms. Besides, it is accepted that the Sm, La, or Mn doped $BiFeO_3$ can extend the modulation period; thus, these elements are less influence on the spin cycloid inside the *R*3*c* rhombohedral symmetry [39]. Therefore, the change of octahedral tilt angle possibly relates to the rearrangement of oxygen atoms around the FeO_6 octahedral in order to modify the cycloid periodicity.

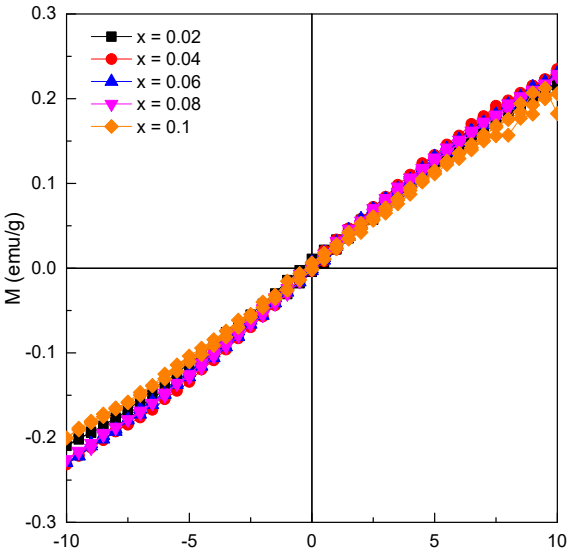

Fig. 5. M-H loops of BSFMO samples measured after synthesis.

It has been observed that the magnetic properties near the morphotropic phase boundary of $BiFeO_3$-based compounds can be varied as a function of time [34, 39, 40]. This effect is attributed to the isothermal structural transition and spin frustration at the phase boundary. To date, there is no study on the variation of magnetic properties of a single structural phase compound. Therefore, it is needed to point out whether the structural defect rearrangement can contribute to the variation of magnetic properties of ceramic compounds. In this work, we measure the $M-H$ loops of BSFMO compounds after two-years synthesis, as shown in Fig. 6(a). It is clear that the hysteresis loops retain the linear magnetic field dependence of magnetization. Fig. 6(b) shows the hysteresis loops of all samples after applying an DC electric field of 40 kV/cm. A slight change in maximum magnetization is observed, but the hysteresis loops clearly show no weak ferromagnetic behavior [41]. Our investigation on the magnetic properties of single phase BSFMO compound confirms that the structural defect rearrangement does not induce the ferromagnetic-like hysteresis loop and weak ferromagnetism as observed previously in the complex structural phase systems [34, 39, 40].

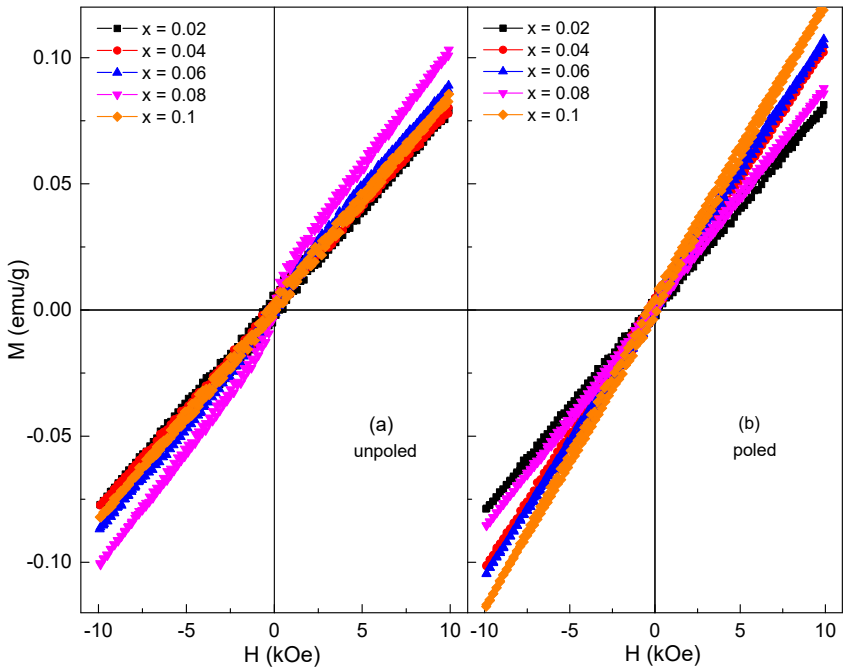

Fig. 6. M-H loops of BSFMO samples measured after 2 years for (a) unpoled and (b) poled in an DC electric field of 40 kV.

IV. CONCLUSIONS

We have investigated the crystal structure, microstructure, and magnetic properties of $Bi_{0.9}Sm_{0.1}Fe_{1-x}Mn_xO_3$ ($0.02 \leq x \leq 0.1$) polycrystalline ceramics. The analysis of crystal structure confirms that all the samples are crystallized in the $R3c$ rhombohedral structure. Raman study reveals the lattice distortion in Mn-substitution samples. The magnetic properties of BSFMO compounds do not improve with the substitution of Mn at Fe site. The studies on the magnetic properties at different time and in an applied electric field show no ferromagnetic-like hysteresis loop, implying that the structural defect rearrangement does not induce the weak ferromagnetism in single structural phase compounds.

ACKNOWLEDGEMENTS

This research is funded by Vietnam National Foundation for Science and Technology Development (NAFOSTED) under grant number 103.02-2019.22, and funded by the Ministry of Education and Training of Vietnam (B2019-TNA-03.VL).

REFERENCES

[1] J. M. Hu, Z. Li, L. Q. Chen, and C. W. Nan, *Nat. Commun.* **2** (2011) 553.
[2] J. M. Hu, L. Q. Chen, and C. W. Nan, *Adv. Mater.* **28** (2016) 15.
[3] V. G. Bhide and M. S. Multani, *Solid State Commun.* **3** (1965) 271.
[4] D. Lebeugle, D. Colson, A. Forget, and M. Viret, *Appl. Phys. Lett.* **91** (2007) 10.
[5] C. Tab Ares-Muñoz, J. P. Rivera, A. Bezinges, A. Monnier, and H. Schmid, *Jpn. J. Appl. Phys.* **24** (1985) 1051.
[6] J. Singh, A. Agarwal, S. Sanghi, M. Yadav, T. Bhasin, and U. Bhakar, *Appl. Phys. A Mater. Sci. Process.* **125** (2019) 156.
[7] D. V. Karpinsky, I. O. Troyanchuk, A. V. Trukhanov, M. Willinger, V. A. Khomchenko, A. L. Kholkin, V. Sikolenko, T. Maniecki, W. Maniukiewicz, S. V. Dubkov, and M. V. Silibin, *Mater. Res. Bull.* **112** (2019) 420.
[8] F. Pedro-García, L. G. Betancourt-Cantera, A. M. Bolarín-Miró, C. A. Cortés-Escobedo, A. Barba-Pingarrón, and F. Sánchez-De Jesús, *Ceram. Int.* **45** (2019) 10114.
[9] S. K. S. Patel, J. H. Lee, M. K. Kim, B. Bhoi, and S. K. Kim, *J. Mater. Chem. C* **6** (2018) 526.
[10] L. Pan, Q. Yuan, Z. Liao, L. Qin, J. Bi, D. Gao, J. Wu, H. Wu, and Z. G. Ye, *J. Alloys Compd.* **762** (2018) 184.
[11] P. T. Phong, N. H. Thoan, N. T. M. Hong, N. V. Hao, L. T. Ha, T. N. Bach, T. D. Thanh, C. T. A. Xuan, N. V. Quang, N. V. Dang, T. A. Ho, and P. T. Tho, *J. Alloys Compd.* **813** (2019) 152245.
[12] D. V. Karpinsky, I. O. Troyanchuk, M. Tovar, V. Sikolenko, V. Efimov, and A. L. Kholkin, *J. Alloys Compd.* **555** (2013) 101.
[13] D. V. Karpinsky, I. O. Troyanchuk, V. Sikolenko, V. Efimov, E. Efimova, M. Willinger, A. N. Salak, and A. L. Kholkin, *J. Mater. Sci.* **49** (2014) 6937.
[14] E. Gil-González, A. Perejón, P. E. Sánchez-Jiménez, M. A. Hayward, J. M. Criado, M. J. Sayagués, and L. A. Pérez-Maqueda, *J. Alloys Compd.* **711** (2017) 541.
[15] Z. Liao, W. Sun, Q. Zhang, J. F. Li, and J. Zhu, *J. Appl. Phys.* **125** (2019) 175113.
[16] A. A. Belik, A. M. Abakumov, A. A. Tsirlin, J. Hadermann, J. Kim, G. Van Tendeloo, and E. Takayama-Muromachi, *Chem. Mater.* **23** (2011) 4505.
[17] K. Shigematsu, T. Asakura, H. Yamamoto, K. Shimizu, M. Katsumata, H. Shimizu, Y. Sakai, H. Hojo, K. Mibu, and M. Azuma, *Appl. Phys. Lett.* **112** (2018) 1.
[18] S. M. Selbach, T. Tybell, M. A. Einarsrud, and T. Grande, Chem. Mater. **21** (2009) 5176.
[19] J. Anthoniappen, W. S. Chang, A. K. Soh, C. S. Tu, P. Vashan, and F. S. Lim, *Acta Mater.* **132** (2017) 174.
[20] M. D. Chermahini, I. Safaee, M. Kazazi, and M. M. Shahraki, *Ceram. Int.* **44** (2018) 14281.
[21] G. S. Arya, R. K. Sharma, and N. S. Negi, *Mater. Lett.* **93** (2013) 341.
[22] V. A. Khomchenko, I. O. Troyanchuk, M. I. Kovetskaya, and J. A. Paixão, *J. Appl. Phys.* **111** (2012) 014110.
[23] S. D. Zhou, Y. G. Wang, Y. Li, H. Ji, and H. Wu, *Ceram. Int.* **44** (2018) 13090.
[24] R. Pandey, C. Panda, P. Kumar, and M. Kar, *J. Sol-Gel Sci. Technol.* **85** (2018) 166.
[25] S. Saxin and C. S. Knee, *Dalt. Trans.* **40** (2011) 3462.
[26] M. Gowrishankar, D. R. Babu, and P. Saravanan, *Mater. Lett.* **171** (2016) 34.
[27] V. A. Khomchenko, D. V Karpinsky, I. O. Troyanchuk, V. V Sikolenko, D. M. Többens, M. S. Ivanov, M. V Silibin, R. Rai, and J. A. Paixão, *J. Phys. D. Appl. Phys.* **51** (2018) 165001.
[28] V. A. Khomchenko, D. V. Karpinsky, L. C. J. Pereira, A. L. Kholkin, and J. A. Paixão, *J. Appl. Phys.* **113** (2013) 214112.
[29] J. Hlinka, J. Pokorny, S. Karimi, and I. M. Reaney, *Phys. Rev. B* **83** (2011) 020101.
[30] J. Bielecki, P. Svedlindh, D. T. Tibebu, S. Cai, S.-G. Eriksson, L. Börjesson, and C. S. Knee, *Phys. Rev. B* **86** (2012) 184422.
[31] Y. J. Wu, J. Zhang, X. K. Chen, and X. J. Chen, *Solid State Commun.* **151** (2011) 1936.
[32] L. Chen, Y. He, J. Zhang, Z. Mao, Y. J. Zhao, and X. Chen, *J. Alloys Compd.* **604** (2014) 327.
[33] C. Ederer and N. A. Spaldin, *Phys. Rev. B* **71** (2005) 060401(R).
[34] P. T. Tho, N. V. Dang, N. X. Nghia, L. H. Khiem, C. T. A. Xuan, H. S. Kim, and B. W. Lee, *J. Phys. Chem. Solids* **121** (2018) 157.
[35] I. O. T. I. Sosnowska, W. Schäfer, W. Kockelmann, K.H. Andersen, *Appl. Phys. A: Mater. Sci. Process.* **74** (2002) S1040.
[36] T. Park, G. C. Papaefthymiou, A. J. Viescas, A. R. Moodenbaugh, and S. S. Wong, *Nano Lett.* **7** (2007) 766.

[37] A. Singh, A. Senyshyn, H. Fuess, S. J. Kennedy, and D. Pandey, *Phys. Rev. B* **89** (2014) 024108.
[38] V. A. Khomchenko, J. A. Paixão, V. V. Shvartsman, P. Borisov, W. Kleemann, D. V. Karpinsky, and A. L. Kholkin, *Scr. Mater.* **62** (2010) 238.
[39] T. H. Le, N. V. Hao, N. H. Thoan, N. T. M. Hong, P. V. Hai, N. V. Thang, P. D. Thang, L. V. Nam, P. T. Tho, N. V. Dang, and X. C. Nguyen, *Ceram. Int.* **45** (2019) 18480.
[40] P. T. Tho, N. X. Nghia, L. H. Khiem, N. V. Hao, L. T. Ha, V. X. Hoa, C. T. A. Xuan, B. W. Lee, and N. V. Dang, *Ceram. Int.* **45** (2019) 3223.
[41] X. X. Shi, X. Q. Liu, and X. M. Chen, *Adv. Funct. Mater.* **27** (2017) 1604037.